Optical characterization of GaN thin film grown on Si(111) by radio-frequency plasma-assisted molecular beam epitaxy

L.S. Chuah, Z. Hassan, H. Abu Hassan

Nano-Optoelectronics Research and Technology Laboratory

School Of Physics, Universiti Sains Malaysia, 11800 Penang, Malaysia

chuahleesiang@yahoo.com, zai@usm.my

Abstract

The wide band gap gallium nitride (GaN) based semiconductor system has great potential for applications in high-power, high-frequency, and high-temperature optoelectronic devices due to its superior properties, such as large breakdown field, high electron mobility, and thermal stability at elevated temperature. In this work, we present the optical characteristics of GaN thin film grown on silicon (Si) substrate by radio-frequency plasma-assisted molecular beam epitaxy (RF-MBE). Micro-photoluminescence (μ-PL) and micro-Raman spectroscopy were used to study the room temperature optical properties of the films. For the PL measurement, an intense and sharp band edge emission peak at 3.40 eV (with the FWHM of 60 meV) and two emission peaks attributed to the defect recombination were observed at 2.89 eV, and 2.26 eV. Raman result showed that the E_2(high) mode of GaN and the E_2(high) mode of the AlN buffer were clearly visible. The PL and Raman results revealed that the GaN epilayer was successfully grown on Si substrates.

1. Introduction

To date, most of the gallium nitride (GaN) films commercially found in the market were grown on sapphire (Al_2O_3) substrates. However, silicon (Si) has shown its potential as an alternative substrate to Al_2O_3 to grow GaN due to its high quality and wide availability as a large diameter and low cost substrate.

MBE is perhaps the most versatile technique available to deposit high purity thin films of metals semiconductors and insulators with very precise layer and composition control. Molecular beam epitaxy (MBE) was developed by Al Cho and J.R. Arthur at AT&T Bell labs in the early 1970s. Since then, it has developed into a sophisticated tool for crystal growth for high performance electronic and optoelectronics devices.

A typical MBE reactor is an ultra-high vacuum chamber wherein high purity source materials are thermally evaporated. The evaporated atoms or molecules have a long mean-free path because of low pressure ($\sim 1 \times 10^{-9}$ torr) inside the chamber. The molecular (or atomic) beams of these evaporated species are directed onto a heated substrate for thin film deposition. Precise control of the source material flux, substrate temperature, and other growth parameters is possible through the use of in-situ and ex-situ measurement and control systems.

MBE growth is carried out under conditions that are governed primarily by kinetics, rather than mass transfer. A thorough understanding of the growth kinetics, especially the surface processes of growth, is a key issue for further improvement of material quality. A series of surface processes takes place during the growth which is schematically illustrated in Fig. 1.
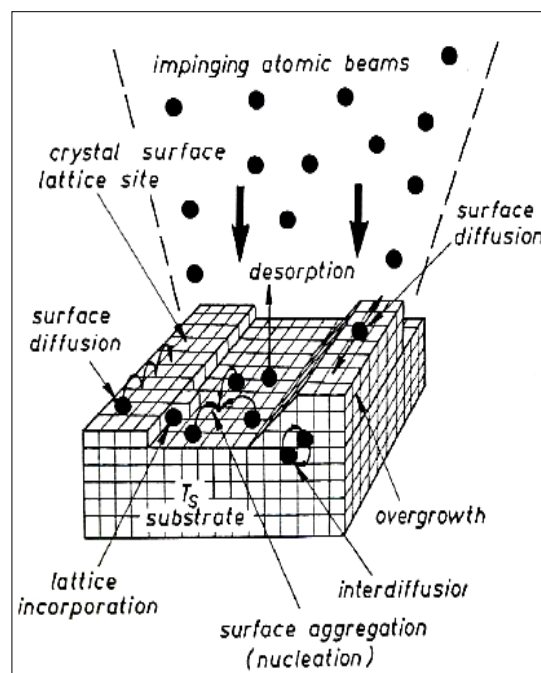

Fig. 1: Schematic illustration of the surface processes during growth in a MBE system (Adopted from Herman and Sitter 1989) [1]

The most important processes are (i) adsorption: atomic or molecules or constituent atoms impinging on the substrate surface and "stick" by overcoming the activation barrier; (ii) incorporation: species bond to the substrate or epilayer by attaching to a dangling bond, vacancy, step edge;

(iii) surface diffusion: species diffuse on the substrate surface to find low energy crystal sites; (iv) decomposition: atoms in the crystal lattice leave the surface after breaking their bond; (v) desorption: species not incorporated into the crystal lattice leave the substrate by thermal re-evaporation [1].

These surface processes during MBE growth are of principal importance, as they define the primary pathways of composition, point-defect concentration and growth-rate control. They play an important role in optimizing growth parameters so as to obtain high-quality structures with planar or periodically modulated interfaces.

To date, most of the gallium nitride (GaN) films commercially found in the market were grown on sapphire (Al_2O_3) substrates. However, silicon (Si) has shown its potential as an alternative substrate to Al_2O_3 to grow GaN due to its high quality and wide availability as a large diameter and low cost substrate [2]. In addition, the use of Si substrates for growth of GaN indicates the possibility of future integration with Si device technology [3]. As a result, we predict a wide array of GaN on Si substrate based devices can be realized in future. Direct growth of a GaN film on Si substrate results in either polycrystal growth or a substantial diffusion of Si into the GaN film. Thin AlN and SiC films have been used as buffer layers for GaN growth on Si substrate [4,5,6].

Vibrational characterization by Fourier transform infrared spectroscopy (FTIR) revealed that the stress in the AlN films deposited on Si (111) substrates was also smaller than AlN films deposited on Si (100) substrates. The lattices in AlN (0001) and Si (111) are both hexagonal, and thus Si (111) can provide matched template for AlN (0001) plane. The lattice mismatch between these two plane is 19% ($d_{Si (111)}$-$d_{AlN (0001)}$/$d_{Si (111)}$, here $d_{Si (111)}$ refers to the Si lattice distance in Si (111) plane; $d_{AlN (0001)}$ refers to the AlN lattice distance in AlN (0001) plane) [6].

The lattice in Si (100) is square, which is unmatched with hexagonal lattice in AlN (0001) plane. The lattice mismatch between AlN (0001) and Si (100) is 42.7% ($d_{Si (100)}$-$d_{AlN (0001)}$/$d_{Si (100)}$, here $d_{Si (100)}$ refers to the Si lattice distance in Si (100) plane) [6]. The larger lattice mismatch between AlN (0001) and Si (100) is a main contribution to the larger strain in the formed films. In the case of GaN layers grown on AlN buffer layer the crystalline quality is much improved because the lattice mismatch between GaN and AlN is only 2.5%. For these reasons, the Si (111) substrate was used.

In this paper, we report on the room temperature micro-photoluminescence (μ-PL) and micro-Raman characteristics of GaN films on AlN buffer layer on Si substrate. The sample was grown by radio-frequency plasma-assisted molecular beam epitaxy (RF-MBE).

2. Experimental details

The film growth has been performed in a Veeco Gen II MBE system. Active nitrogen was produced using a Veeco Unibulb inductively coupled plasma source. In situ RHEED measurements were performed using a 15 keV electron gun. The base pressure in the system was below 5 x 10^{-11} Torr. Three inch n-type Si (111) wafer was used for the substrate of wurtzite GaN growth. Prior to loading into MBE chamber, the Si (111) wafers (resistivity < 0.02 ohm-cm, n-type) were ultrasonically degreased in solvents and etched in buffered HF.

The substrate is mounted on a block, which is then secured onto the continual azimuthal rotation (CAR) assembly. The CAR assembly rotates and heats the substrate during growth. Substrate rotation helps growth uniformity from substrate center to the edges. Substrate temperature is monitored using two independent systems: a thermocouple fitted behind the block, and an external infrared pyrometer. An ionization gauge is also fitted on the CAR. The CAR can be rotated such that the ionization gauge can be placed at the substrate growth position.

In this position, the ionization gauge can read the beam equivalent pressure (BEP) of the incident flux. This is one of the ways to calibrate the source flux, but is used mainly to determine and set the group-V flux. Additionally, the RHEED technique is also used for verification of thermal desorption of the native oxides from the substrate surface, and surface temperature determination. The native oxides formed on certain substrates thermally desorb at a fixed temperature.

In the growth chamber, the substrates were outgassed for 10 min at 900 °C prior to growth. The plasma was operated at typical nitrogen pressure of 1.5×10^{-5} Torr under a discharge power of 300 watts. A few monolayers of Ga were deposited on the substrate for the purpose of removing the SiO_2 by formation of GaO_2. After a few minutes, a reflection high energy electron diffraction (RHEED) reconstruction with prominent Kikuchi lines is then observed that turns into clean Si (111) surfaces at 750 °C, as shown in Fig. 2.
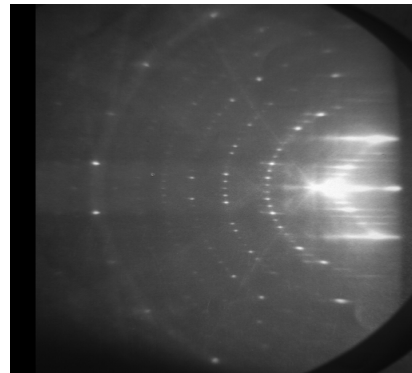

Fig. 2: RHEED diffraction indicates clean Si(111) surface with prominent Kikuchi lines.

Then a few monolayers of Al is deposited on Si(111) prior to an AlN buffer layer growth. AlN deposition is started by opening both Al (cell at 1120 °C) and N shutters simultaneously. The role of this layer is to improve the crystalline quality of the latter doped GaN layer. The unintentionally doped n-type GaN film grown on Si(111) substrate was used in this study. The thickness of GaN film is about 0.06 μm with carrier concentration of ~ 4×10^{18} cm^{-3} as determined by Hall Effect measurement.

Micro-Raman and photoluminescence (PL) measurements were performed at room temperature using Jobin Yvon HR800UV system. Argon ion (514.5 nm) laser and He-Cd (325.0 nm) laser were used as excitation sources for Raman and PL measurements respectively. To focus the laser on the sample surface, microscope objective lenses 100× and UV40× were employed for Raman and PL measurements respectively. The diameter of the laser spot on the samples was around 20 μm. The emitted light was dispersed by a double grating monochromator with 0.8 m focal length and equipped with 1800 grove/mm holographic plane grating. Signals were detected by a Peltier cooled charge-coupled-device (CCD) array detector. Before the micro-Raman and micro-PL measurement, high quality single crystal silicon sample (with the zone-center-mode at 520.70 cm^{-1}) was used to calibrate the system. The full width at half-maximum (FWHM) of the Si Lorentzian peak width was ~ 3 cm^{-1}. The essential parameters of the Raman and PL peaks were determined by using curve fitting software with Gaussian and Lorentzian model.

3. Results and discussion

Fig. 3 shows how the RHEED pattern changes during buffer layer (AlN) growth. Fig. 3(a) exemplifies typical RHEED images at few monolayers of Al. Figs. 3(b)-(d) show the RHEED images with 90sec, 5min and 15min of AlN buffer layer growth. After 5 min of AlN buffer growth, a stable pattern which is different from Si(111) was formed. In this work, the sample was grown under Ga-stable conditions (Ga/N flux ratio greater than 1) that result in GaN growth, as shown in Fig. 4. Growth of GaN by MBE utilizing high temperature buffer layer on Si(111) substrate almost always grow as Ga-polar material. The films were found to be of good crystallinity as indicated by the streaky RHEED pattern indicating an atomically smooth surface. It is difficult to perform experiments on both polarities of GaN using MBE, as in this study, when it is only possible to nucleate one polarity.

For GaN films grown by MBE, the most common impurity is carbon. Besides that, the samples may most probably be contaminated by residual Si (from the Si substrate). In addition, nitrogen vacancies ($N_{Ga\ site}$) and gallium vacancies ($Ga_{N\ site}$) are also two common defects in the GaN films. This led to the suggestion that the GaN films contained these defect-
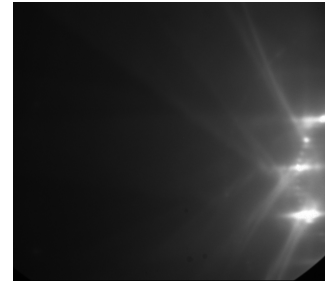
related levels in the band gap that may be the source of radiative recombination centres and leading to below band gap optical emission. For this reason, PL spectroscopy is a good characterization tool to identify the appearance of defect-related levels (or defect induced luminescence) in the sample.
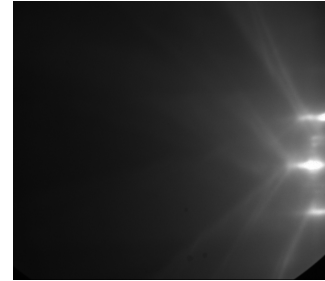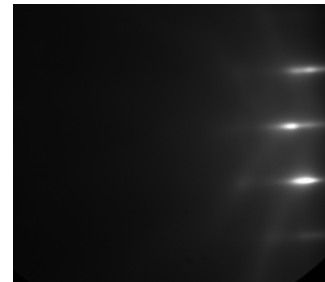

(a)
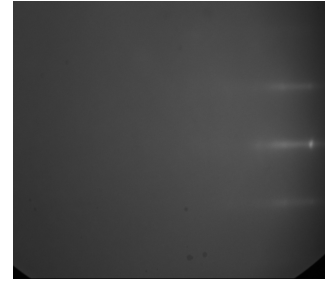
(b)

(c)

(d)

Fig. 3: (a) Typical RHEED image at few monolayers of Al before AlN buffer layer growth. (b)-(d) show the RHEED images with 90sec, 5min and 15min of AlN layers.

Fig. 4: RHEED image of the GaN layers.

Fig. 5 shows the PL spectrum at room temperature for GaN/AlN/Si. In order to determine the peaks position and the FWHM as accurately as possible, the PL spectra is fitted by Gaussian/Lorentzian function. It can be seen that the fitting of theoretical spectra to the measured spectra is good in each case. From Fig. 1, a strong near band edge emission at 364.54 nm (3.40 eV) having a FWHM of 6.46 nm (60 meV) was observed. This value is comparable to those quoted by Oshinsky *et al.* [7] and Zhang *et al.* [8]. In addition, two luminescence peaks attributed to the defect recombination, namely, the blue (BL), and orange-yellow (YL) were observed at 428.69 nm (2.89 eV), and 548.88 nm (2.26 eV) respectively.
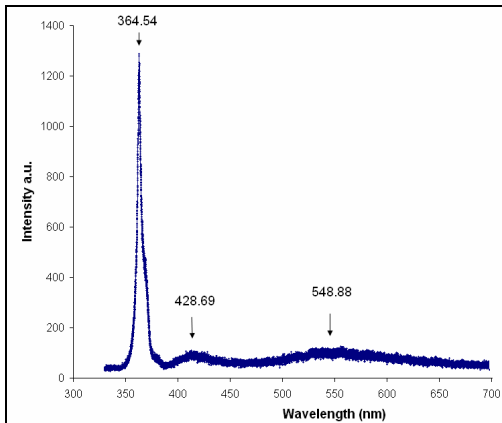

Fig. 5: Room temperature PL spectrum of GaN thin film on AlN buffer layer grown on Si substrate.

Two of these PL bands, namely, the BL and YL are often found in nominally undoped GaN [9,10]. The luminescence mechanism of these bands is believed to be due to $N_{Ga\ site} - C_{N\ site}$ deep donor-shallow acceptor transition and $Si - Ga_{N\ site}$ shallow donor-deep acceptor transition [11-13] respectively. The RL is rarely observed in n-type GaN PL studies. Nevertheless, the observation of the RL in GaN has been reported by several researchers. The origin of this

peak could be a result of transition between a $N_{Ga\ site} - Ga_{N\ site}$ deep donor-deep acceptor state [14-17].

Raman scattering occurs essentially as a result of modulation of the electronics polarizability induced by various elementary excitations in solids such as phonons. Fig. 6 shows the Raman scattering spectrum for the laser light incident normal to the surface of the GaN epilayer. Before analyzing the Raman spectrum, let us recall that GaN crystallizes in a wurtzite structure with four atoms in the unit cell and belongs to the space group C_{6v}^{4} ($C6_3\,mc$). The phonon dispersion of the hexagonal structure along [0001] ($\Gamma \rightarrow A$ in the Brillouin zone), is shown schematically in Fig. 7. In the hexagonal structure, group theory predicts two A_1, two E_1, two E_2 and two B_1 modes at the Γ point [18]. Among them, one set of A_1 and one E_1 modes are acoustic vibrations. The E_2 modes are Raman active, the A_1 and the E_1 modes are both Raman and infrared active, and the B_1 modes are silent. The six Raman active phonons—i.e., A_1(TO), A_1(LO), E_1(TO), E_1(LO), E_2(low) and E_2(high) - can be observed for first-order Raman scattering. The first-order phonon Raman scattering is caused by phonons with wavevector $k \sim 0$ (Γ point) because of a momentum conservation rule in the light scattering process.
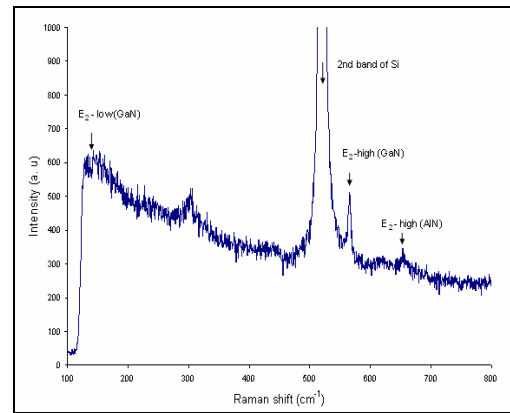

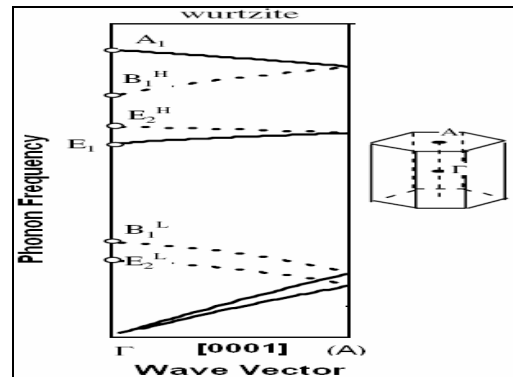Fig. 6: Room temperature micro-Raman spectrum of GaN/Si.

Fig. 7: Schematic representation of the phonon dispersion. Phonon branches along [0001] in the wurtzite structure.

In this work, micro-Raman scattering experiments were carried out in the $z(x, \text{unpolarized}) \bar{z}$ scattering configuration. Here, the Porto's notation is used for scattering geometries with z parallel to wurtzite c axis, and (x, unpolarized) refers to the polarization of the incident and scattered light. Under this configuration, the allowed zone-center phonon modes that can be detected for wurtzite structure layer will be $A_1(LO)$, $E_2(low)$, and $E_2(high)$, unless there are some disoriented microstructures. The atomic displacement scheme of these optical modes is shown in Fig. 8. The A_1 modes give atomic displacements along the c-axis, while the others, the E_2 give atomic displacements perpendicular to the c-axis.

In general, an E_2 phonon frequency shift to higher frequencies in comparison to that of stress-free samples denotes the presence of compressive strain while a shift to lower frequencies indicates tensile strain and this can be correlated to the thermal residual strain in the films. The E_2 (high) mode in the Raman spectra can be used to estimate the stress because it has been proven to be particularly sensitive to biaxial stress in samples.

A room temperature micro-Raman spectrum of GaN/AlN/Si is displayed in Fig. 6. A strong band is observed at 520.39 cm^{-1} which is the contribution from the Si(111) substrate, and a band at ~ 300 cm^{-1} due to the acoustic phonons of Si. However, the incorporation of the unintentionally n-doped has lead to high background intensities in the low wavenumber (100 – 250 cm^{-1}) region. This n-type doping is generally caused by nitrogen vacancies in the crystalline structure, which are expected to be shallow donors in GaN films. Oxygen is commonly found as an impurity in GaN layers, and contributes to the n-type carrier concentration.
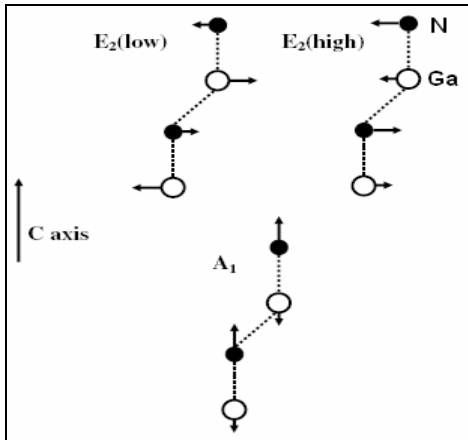

Fig. 8: Atom vibration modes in hexagonal GaN with the c axis upward.

The dominant E_2 (high) phonon mode of GaN appears at 565.81 cm^{-1}, which is nearly comparable to the best-reported result in the literatures [19]. The E_2 (high) phonon mode of AlN appears at 653.40 cm^{-1} and deviates from the standard value of 655 cm^{-1} for an unstrained AlN [20]. The shift of E_2 (high) modes of GaN to lower frequencies with respect to the standard value of strain-free bulk (568 cm^{-1}) implies a biaxial tensile stress in the epilayer. The consequences of large lattice and thermal expansion coefficient mismatch between GaN and Si, 5.59 and 2.59x10^{-6} K^{-1} (300K) respectively, result in high dislocation density films and also large tensile stress during cooling from the growth temperature to room temperature of GaN epitaxy [21]. The redshift can be easily understood according to the configurations of phonon modes, as shown in Fig. 8, in which the c axis points upward. For example, the E_2 (high) mode corresponds to the atomic oscillation in the c plane [18].

4. Conclusions

In summary, we have reported the PL and Raman optical characteristics of GaN film grown on Si with AlN buffer layer by RF-MBE. The grown sample exhibits very streaky RHEED patterns. Micro-Raman result showed that all the allowed Raman modes of GaN and AlN were clearly visible and the Raman modes frequencies of GaN are in good agreement with Raman data for bulk single crystals. However, the tensile strain in the films has caused a red shift of the E_2 (High) mode of GaN. For the micro-PL measurement, an intense and sharp band edge emission peak as well as two defect-related luminescence band was observed at 364.58 nm, 428.69 nm, and at 548.88 nm respectively.

Acknowledgement

References

[1] M. A. Herman, H. Sitter, "*Molecular Beam Epitaxy, fundamental and current status*", Springer-Verlag Berlin Heidelberg New York, 1989.

[2] J.W. Yang, A. Lunev, G. Simin, A. Chitnis, M. Shatalov, M.A. Khan, J.E. Van Nostrand, R. Gaska, Appl. Phys. Lett. 76, 273 (2000).

[3] A. Dadgar, J. Christen, T. Riemann, S. Richter, J. Blaesing, A. Diez, A. Krost, A. Alam, M. Heuken, Appl. Phys. Lett. 78, 2211 (2001).

[4] P.W. Deelmann, R.N. Bicknell-Tassius, S. Nikishin, V. Kuryatkov, H. Temkin, Appl. Phys. Lett. 78, 2172 (2001).

[5] Y. Hiroyama, M. Tamura, Jpn. J. Appl. Phys. 37, L630 (1998).

[6] J. X. Zhang, H. Cheng, Y.Z. Chen, A. Uddin, Shu Yuan, S.J. Geng, S. Zhang, Surf. And Coat. Tech.198, 68 (2005).

[7] A. Oshinsky, S. Gangopadhyay, J.W. Yang, R. Gaska, D. Kuksenkov, H. Temkin, I.K.

Shmagin, Y.C. Chang, J. F. Muth, R.M. Kolbas, Appl. Phys. Lett. 72, 551 (1998).

[8] X. Zhang, S. J. Chua, P. Li, K.B. Chong, Z.C. Feng, Appl. Phys. Lett. 74, 1984 (1999).

[9] U. Rossler, H.R. Trebin, Phys. Rev. B 23, 1961 (1981).

[10] L.C. Andreani, F. Bassani, Phys. Rev. B 41, 7536 (1990).

[11] D.M. Hofmann, D. Kovalev, G. Steude, B.K. Meyer, A. Hoffmann, L. Eckey, R. Heitz, T. Detchprm, H. Amano, I. Akasaki, Phys. Rev. B 52, 16702 (1995).

[12] J. Neugebauer, C.G. Van de Walle, Appl. Phys. Lett. 69, 503 (1996).

[13] W.G. Perry, M.B. Bremser, R.F. Davis, J. Appl. Phys. 83, 469 (1998).

[14] D.M. Hofmann, B.K. Meyer, H. Alves, F. Leiter, W. Burkhard, N. Romanov, Y. Kim, J. Krüger, E.R. Weber, phys. stat. sol. (a) 180, 261 (2000).

[15] S. Nakamura, N. Iwasaki, M. Senoh, T. Mukai, Jpn. J. Appl. Phys. 31, 1258 (1992).

[16] W. Götz, L.T. Romano, B.S. Krusor, N.M. Johnson, Appl. Phys. Lett. 69, 242 (1996).

[17] U. Kaufmann, M. Kunzer, H. Obloh, M. Maier, Ch. Manz, A. Ramakrishnan, B. Santic, Phys. Rev. B 59, 5561 (1999).

[18] F. C. Wang, C.L. Cheng, Y.F. Chen, C.F. Huang, C.C. Yang, Semicon. Sci. Technol. 22, 896 (2007).

[19] S.A. Nikishin, N.N. Faleev, V.G. Antipov, S. Francoeur, L. Grave De Peralta, G.A. Seryogin, H. Temkin, T. I. Prokofyeva, M. Holtz, S.N.G. Chu, Appl. Phys. Lett. 75 , 2073 (1999).

[20] T. Prokofyeva, M. Seon, J. Vanbuskirk, M. Holtz, S.A. Nikishin, N.N. Faleev, H. Temkin, S. Zollner, Phys. Rev. B 63, 125313 (2001).

[21] B.J. Skrommea, K. Pallea, C.D. Poweleitb, H. Yamanec, M. Aokic and F.J. DiSalvod, J. Cryst. Growth 246, 299 (2002).